RZ 3549 (# 99505) 01/12/004
Mathematics & Physics 12 pages

Research Report

Birefringence Control and Manipulation in SiliconOxyNitride

Folkert Horst[a], Bert Offrein[a] Roger Dangel[a], Dorothea Wiesmann[a], Ton Koster[b], and Gian-Luca Bona[a]

IBM Research GmbH
Zurich Research Laboratory
8803 Rüschlikon
Switzerland

[b]Currently at NKT Integration, Blokken 84, DK-3460 Birkerd, Denmark.

Birefringence Control and Manipulation in SiliconOxyNitride

Folkert Horst*[a], Bert Offrein[a], Roger Dangel[a], Dorothea Wiesmann[a],Ton Koster[b], Gian-Luca Bona[a]
[a]IBM Zürich Research Laboratory, Säumerstrasse 4, CH-8803 Rüschlikon, Switzerland.
[b]currently with NKT – Integration, Blokken 84, DK-3460 Birkerød, Denmark.

ABSTRACT

This paper describes methods to control and manipulate birefringence in SiliconOxyNitride waveguides and devices. Each method is demonstrated by measurements on example devices. The methods and devices that will be covered are:

- Reduction of heater induced birefringence in a dynamic gain equalizer by heater design or etched trenches.
- Reduction of polarization mode dispersion in a tunable dispersion compensator by UV trimming of residual waveguide birefringence.
- Polarization conversion using integrated optical half-wave-plates, fabricated by etching trenches at one side of a waveguide.
- Polarization splitting using waveguide sections with specified birefringence, obtained by etched trenches at both sides of the waveguide.

Keywords: Integrated optics, SiON, polarization, birefringence, stress

1. INTRODUCTION

For the design and production of modern integrated optical devices, a precise knowledge of polarization effects in the optical waveguide technology is needed. On one side, this knowledge can be used for the elimination of unwanted polarization effects like polarization dependent loss (PDL) and polarization mode dispersion (PMD) from devices that should be polarization insensitive. On the other side, the polarization effects can also be enhanced. Optical waveguides with strong polarization sensitivity are useful for building devices for PMD characterization, simulation and control, and for applications using polarization diversity schemes. Such devices for various kinds of polarization management are in growing demand due to increasing fiber optical network bit-rates.
In this paper, we will present examples, realized in SiliconOxyNitride (SiON) waveguide technology, that demonstrate both the elimination of unwanted polarization effects, and the use of enhanced polarization effects. On the one side, we will focus on the reduction of PDL in tunable optical gain equalizers and the reduction of PMD in tunable dispersion compensators. On the other side we will present optical building blocks for polarization splitting and rotation that can be used to realize polarization diversity schemes and to build devices for fiber PMD control.

2. SION WAVEGUIDE TECHNOLOGY

2.1. Waveguide fabrication and geometry

A drawing, not to scale, of the geometry of the SiON waveguides [1] is shown in Fig. 2.1. The fabrication of these waveguides starts with a silicon substrate with a top layer of about 15 µm of thermally oxidized SiO_2. On this substrate, a 2 µm thick core layer of SiON is grown by PECVD. The waveguide ridges are etched into this core layer using RIE. The top cladding of the waveguide is again

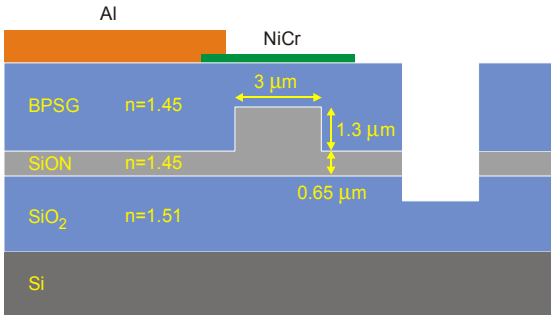

Fig. 2.4: Cross-section of the SiON waveguide structure.

* fho@zurich.ibm.com.

grown by PECVD and consists of BPSG (Boron and Phosphor doped Silica Glass).
For tunable devices, Nickel-Chromium heaters and Aluminum leads for contacts can be deposited on top of the waveguides, using sputtering and lift-off procedures. For tuning of the stress or the power efficiency of the heaters, trenches can be etched adjacent to the waveguides using a RIE process. These structures are shown in Figures 2.2 and 2.3, which give a side by side comparison of the mask layout and the fabricated structures.

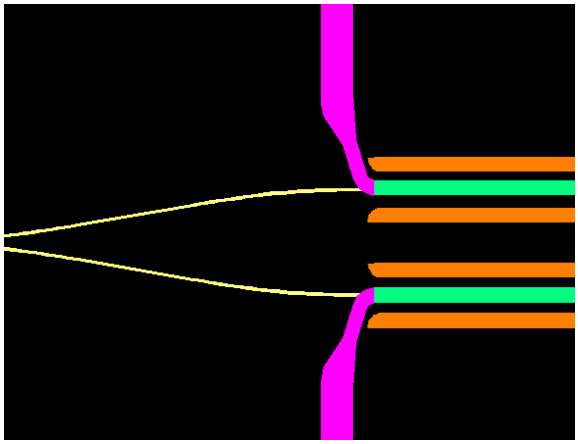

Fig. 2.2: Mask layout, showing waveguides (yellow), heaters (green), leads (magenta) and trenches (orange).

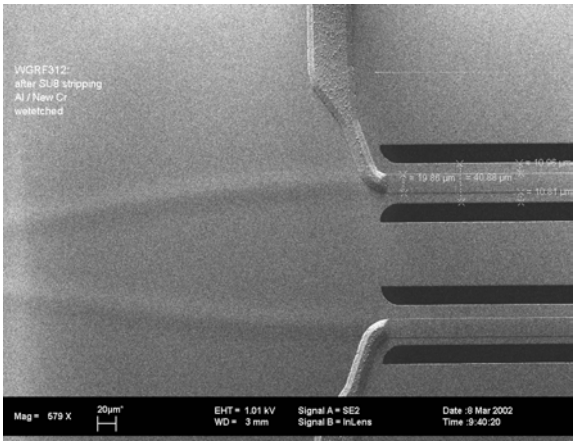

Fig. 2.3: SEM picture of actual structure.

2.2. Origins of waveguide birefringence

The birefringence in the SiON waveguides originates from two contributions:

- Geometrical birefringence: The asymmetrical cross-section of the waveguide leads to a difference in effective index of refraction between TE and TM polarized waveguide modes. For the geometry and core materials of the waveguides discussed here this results in a geometrical birefringence of:
  $\Delta N_{eff,geo} = N_{eff,TM} - N_{eff,TE} = -6.4 \cdot 10^{-4}$.
- Stress birefringence: Although the applied waveguide materials do not display inherent material birefringence, they are subject to directional stress. The stresses arise from the different coefficients of thermal expansion (CTE) of the different layers, including the heater layer, combined with the elevated process temperatures. Because the waveguide structure can freely expand in the vertical direction but is strongly clamped in the horizontal direction by the substrate, the stress becomes strongly directional. Via the elasto-optical effect, this directional stress leads to birefringence.

2.3. Birefringence reduction in passive waveguides

To achieve low birefringence in the passive waveguides, the geometrical birefringence should be counterbalanced by the stress birefringence. Here, the BPSG upper cladding material offers the required degree of freedom to tune the stress. By adjusting the Boron and Phosphor content of this glass, the CTE of the material can be manipulated and at the same time the index of refraction kept constant. For the passive SiON waveguides, the process temperatures and BPSG composition are chosen such that the stress birefringence almost cancels the geometrical birefringence and the overall birefringence is very small: $|\Delta N| < 1 \cdot 10^{-4}$.

2.4. Heaters

Most wavelength selective integrated optic devices are based on the interference between light traveling through an active waveguide branch and light traveling through a reference branch. When the active branch is longer of shorter than the reference branch, the length difference leads to a wavelength-dependent phase shift between the two signals, thus generating wavelength-dependent interference patterns that are used to realize the filter functionality. To make a device tunable, a heater can be deposited on top of the active waveguide branch. By heating, the effective refractive index of the waveguide is changed, which generates an extra phase shift of the light in the waveguide. A 2 mm long heater covers a phase shift range of more than 2 π radians and needs a maximum heater power of 600 mW.

In the unheated, passive state the extra heater layer changes the stress distribution around the waveguide core a little, which leads some to waveguide birefringence. However, this birefringence is easily compensated by adding a dummy heater on the reference waveguide branch. Although the absolute phase of the light leaving the waveguide branches may now be different for TE compared to TM polarized light, the phase delay between the two branches is the same for both polarizations, leading to polarization independent behavior of the device.

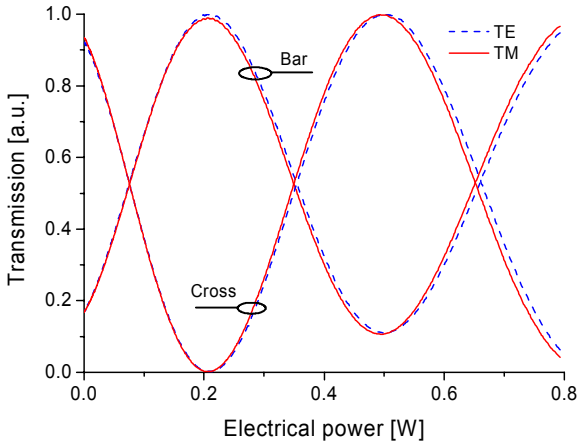

Fig. 2.4: Heater tuning of a single Mach-Zehnder interferometer, showing the difference in tuning efficiency of TE compared to TM polarized light.

When heated, the stress applied by the heater layer changes due to its different CTE relative to the substrate and more importantly, the heating induces temperature gradients in the glass layers close to the waveguide core which changes the stress distribution. This results in a heater induced birefringence (HIB) which manifests itself in a difference in tuning efficiency for the different polarizations of the light. This effect is visible in Fig. 2.4, in the shift of the tuning curves for TE and TM polarized light for higher tuning powers. These curves were measured on a single balanced Mach-Zehnder interferometer. In Section 3, we will show some methods that can be used to minimize HIB in actual devices.

2.5. Trenches

By etching trenches on both sides of the waveguides, they can expand in the horizontal direction, and a large part of the stress that resulted from the difference in CTE between substrate and waveguide layers disappears [2, 3]. This disrupts the balance between geometrical and stress birefringence, and a waveguide with strong birefringence results. However, also the stresses responsible for the generation of HIB can relax. This is one of the possible methods to reduce HIB, as will be shown in Section 3.
Etching of trenches can also be useful to locally induce birefringence, as will be shown in Section 6, where it is used for the fabrication of integrated optical polarization splitters.

An interesting effect arises when a trench is etched on only one side of the waveguide [3]. In this case, the stress in the horizontal direction partly relaxes, at the expense of generating a vertical component. The resulting stress has a directional component that is tilted out of the horizontal plane. The resulting waveguide birefringence also has its fast and slow axes tilted. This effect is discussed in more detail in Section 5, where it is used for the construction of an integrated optical polarization converter.

3. REDUCTION OF POLARISATION DEPENDENT LOSS (PDL) IN A DYNAMIC GAIN EQUALIZER

3.1. Dynamic gain equalizer

The Dynamic Gain Equalizer (DGE) [4] that will be discussed in this example is based on a 7-stage Finite Impulse Response (FIR) lattice filter [5]. This lattice filter consists of a concatenation of 8 variable couplers and 7 tunable delay lines. A schematical layout of such a lattice filter is shown in Fig. 3.1. A 7-stage lattice filter has a periodic filter function with a repetition period or Free Spectral Range (FSR) that is determined by the length difference in one delay line. The shape of the filter function within one period can be specified up to the 7^{th} Fourier component. The magnitudes and phases of the 0^{th} to 7^{th} Fourier component (8 magnitudes and 7 relative phases) are controlled by the 15 heater currents, where it must be noted that the relation between currents and Fourier components is quite complicated [6].

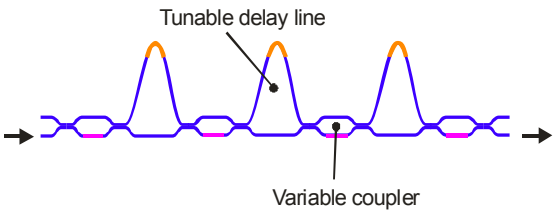

Fig. 3.1: Schematic layout of a lattice filter, here shown with only three stages.

For the actual layout of the lattice filter, we folded the device to have all fiber connections on one side and obtain a compact die, as is shown in Fig. 3.2.

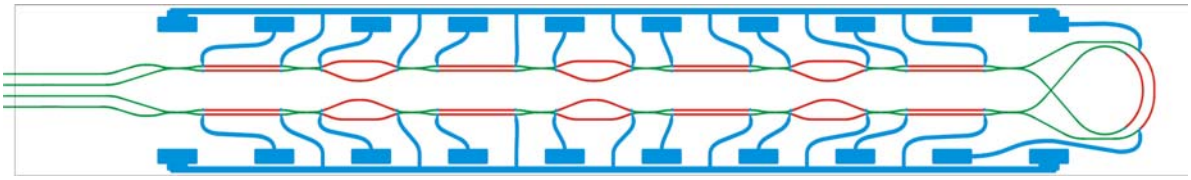

Fig. 3.2: Die layout of a 7-stage folded gain equalizer. The die size is 32 x 4 mm.

3.2. PDL and Heater Induced Birefringence

The main contribution to PDL in the gain equalizer is the result of heater-induced birefringence (HIB). This is a consequence of the large FSR of the device, which is set at 40 nm, the width of the gain region of an Erbium doped fiber amplifier (EDFA). With an FSR of 40 nm, a phase shift of 2 π radians in the delay arms corresponds to a wavelength shift over a full period of 40 nm of the filter curve. When this phase shift is generated by the heaters, an HIB-induced difference in heating efficiency of 2% between TE and TM polarization will result in a wavelength shift of 0.8 nm between the filter curves for the two polarizations. The steepest filter curve slope of the dynamic gain equalizer is of the order of 3 dB/nm. With a polarization dependent wavelength shift of 0.8 nm, this leads to a PDL of the order of 2.5 dB.
As discussed in Section 2.4, HIB results from the temperature dependency of the stress around the waveguide core. We pursued two different methods to reduce this temperature dependency. For the first method, we tried to compensate the temperature-dependent stress in the core SiO_2 and SiON layers by stress of the opposite sign, generated by the heater stripe itself. The second method uses trenches to release the temperature-dependent stress.

3.3. HIB compensation by the heater

When the waveguide is heated, it expands more than the cool substrate, leading to compressive stress on the waveguide. However, the heater itself expands even more than the waveguide and pulls on the waveguide region, generating tensile stress. When the heater pull would be strong enough, both temperature-dependent stress contributions could in principle cancel each other, resulting in negligible HIB.
The force exerted by the heater can be varied by changing heater width, thickness and/or material. However, it must be taken into account that these variations can affect heater resistance, durability and efficiency as well.

We measured the influence of heater material, width and thickness using simple symmetric Mach-Zehnder interferometers as test devices. Test curves from one device are shown in Section 2, in Fig. 2.4. They show heater tuning of one Mach-Zehnder interferometer for TE and TM polarization, clearly demonstrating the difference in tuning efficiency. These measurements were repeated on a large number of devices, with different heater materials, widths and thicknesses. The results are shown below. Fig. 3.5 compares two different heater materials: Chromium, which has a CTE $6.5 \cdot 10^{-6}$ and Nickel-Chromium, which has a CTE of $14.5 \cdot 10^{-6}$. Fig. 3.6 then shows, for the optimum material NiCr, the dependencies of HIB on heater thickness and width.

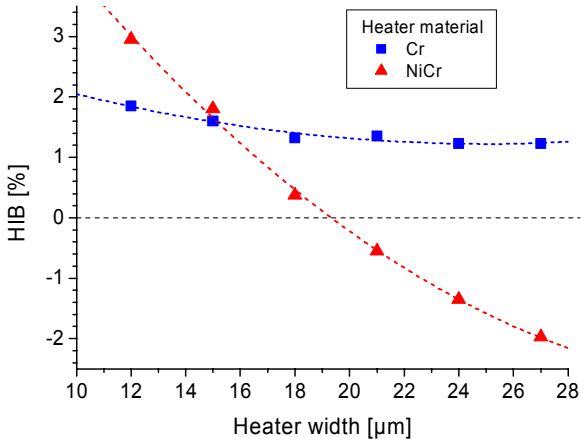

Fig. 3.5: Measured HIB, as a function of heater width and material. Heater thickness is 600 nm.

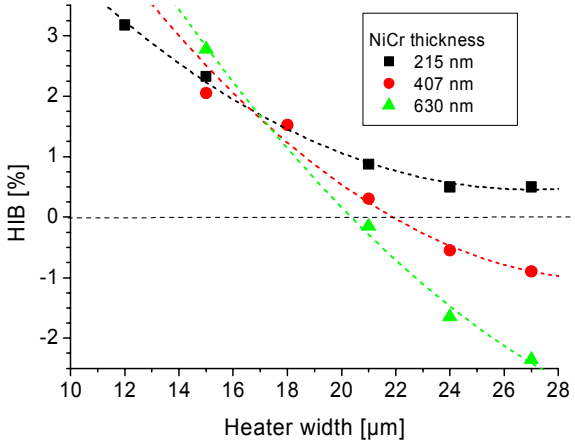

Fig. 3.6: Measured HIB, as a function of heater width and thickness.

These measurements show that it is possible to reduce the HIB to zero using heater compensation, when the CTE of the heater material and the heater width and thickness are large enough. A disadvantage of this method is the low resistance of the resulting heater, which needs very high currents for a given desired heating power. Also we found considerable variations between measurements, which we attributed to a strong dependency of the HIB compensation on the heater process parameters, and on upper cladding thickness as well. A final concern is that the strong stresses that are generated by the heater might lead to peel-off of the heater and failure on the long term.

3.4. HIB reduction using trenches

The temperature-dependent stress and with it the HIB, would disappear when the waveguide core layers could also release their stress in the horizontal direction. This situation can be achieved reasonably well by etching trenches at both sides of the waveguide core, as discussed in Sec. 2.5. At the same moment, also the passive stress, and with it the stress birefringence that balances the geometrical birefringence will be released. The resulting waveguide will have considerable (geometrical) birefringence. However, this passive birefringence can easily be compensated by also etching trenches of equal length around the waveguide in the reference branch of the interferometer, as discussed before in Sec. 2.4.

We used a large number of symmetric Mach-Zehnder interferometers to measure the effect of trench width, trench gap (distance between the inner walls of the left and right trenches) and heater width on the HIB. In these

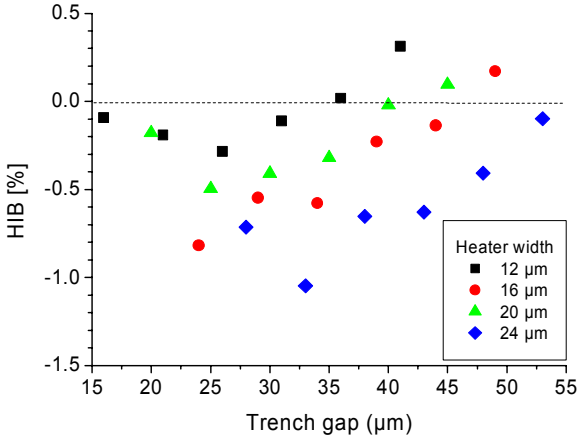

Fig. 3.7: Measured HIB, as a function of heater width and trench gap (distance between inner walls of the trenches).

runs we used chromium heaters. The heater width was again taken into account, because in this situation there is a mix of two effects: HIB reduction by (partial) stress release by the trenches, but also some stress compensation by heater expansion. We found that as long as there is a trench, the HIB reduction is almost independent on trench width. Fig. 3.7 shows the dependency of the HIB on the more important parameters: trench gap and heater width. These curves clearly show that it is possible to minimize HIB using etched trenches. The optimum parameters lie in a comfortable range, with a trench width that is close to our previous design and with the trenches not too close to the waveguide core. Also the dependency on process parameters is small which makes this a simple and reliable method for HIB reduction. The main disadvantage of HIB reduction by trench etching is the extra process step that is required. However, given the other advantages, we prefer this method over HIB reduction by heater design.

3.5. Results

The effect of HIB reduction on device performance is demonstrated in Figures 3.8, 3.9 and 3.10. The first figure shows the wavelength response of a tunable asymmetrical Mach-Zehnder interferometer. This device is similar to one tunable delay line stage of the dynamic gain equalizer (see Fig. 3.1). Using the tuning heater, the wavelength response can be shifted over more than 40 nm. Figure 3.9 shows the wavelength mismatch between the two polarizations, as a function of heater wavelength tuning, for both optimized and un-optimized devices. In the un-optimized device the mismatch between the device response for TE and TM polarization increases to up to 0.7 nm, due to a HIB of approximately 1.2 %. In the optimized device the HIB is reduced to less than 0.2 % and the total polarization mismatch, including passive birefringence, stays below 0.15 nm.

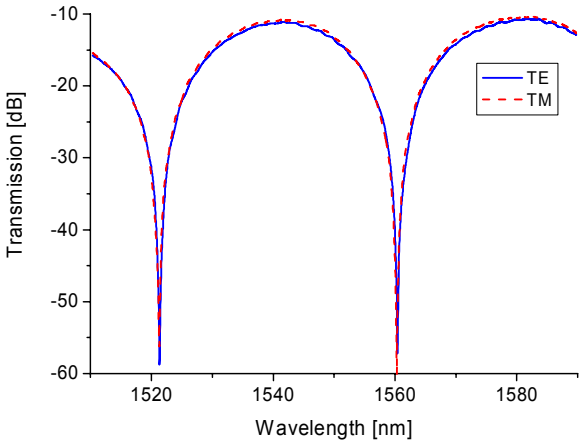

Fig. 3.8: Wavelength response of a single asymmetrical Mach-Zehnder interferometer.

Fig. 3.10 shows the result when the same optimizations are applied to a complete gain equalizer. This curve was taken for evaluation of PDL performance alone, so no particular care was taken to obtain a smooth curve. The measurement shows that for curves with an attenuation of up to 15 dB, the PDL now stays well below 1 dB. When the attenuation is limited to 10 dB, the PDL stays below 0.5 dB. This is a considerable improvement over previously measured values of over 2 dB PDL for the steeper attenuation curves

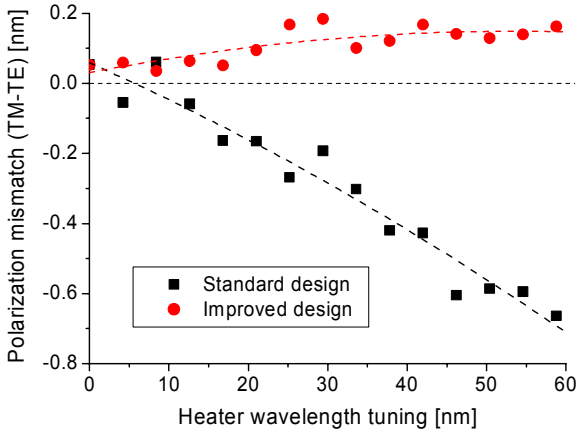

Fig. 3.9: Polarization mismatch as a function of wavelength tuning, in a single asymmetrical Mach-Zehnder interferometer.

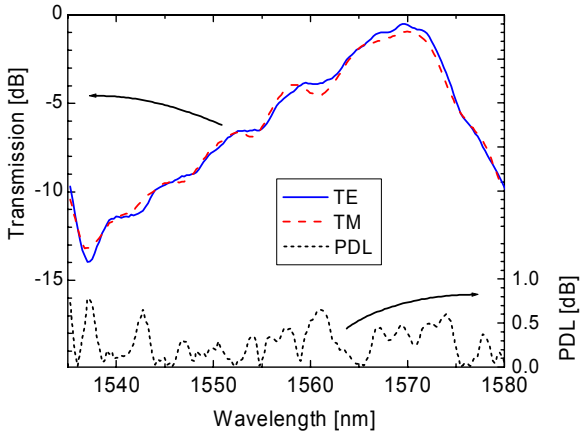

Fig. 3.10: Variation of the attenuation curve with polarization and resulting PDL of an improved dynamic gain equalizer.

4. REDUCTION OF POLARISATION MODE DISPERSION (PMD) IN A TUNABLE DISPERSION COMPENSATOR

4.1. Tunable dispersion compensator

The tunable dispersion compensator is, like the dynamic gain equalizer discussed in the previous section, based on a FIR lattice filter. However, in this case the device has only 6 stages, and more importantly, the relative delay in the delay arms is chosen much larger in order to achieve an FSR of only 0.8 nm or 100 GHz. Because the chromatic dispersion generated by an FIR filter scales with $1/FSR^2$, it is increased from a negligible value for the Gain Equalizer, to a significant and usable property for this filter [7].

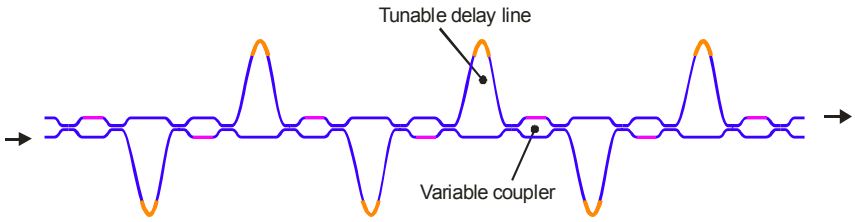

Fig. 4.1: Schematic layout of the tunable dispersion equalizer.

The schematic layout of the filter is shown in Fig. 4.1. In this case a layout was chosen where the long arms of the delay lines lie on alternating sides [7]. This layout helps with the folding of the device, as can be seen in the drawing of the die layout of the device, shown in Fig. 4.2. Examples of group delay curves that can be achieved with the tunable dispersion compensator [8] are shown in Fig. 4.3.

4.2. Polarization Mode Dispersion

The main degrading effect in the dispersion compensator is the Polarization Mode Dispersion (PMD), the variation of the group delay curve with the polarization of the light. As with the gain equalizer, the main contribution to the PMD comes from the polarization dependent wavelength shift of the group delay curve, due to birefringence in the delay line arms. However, in this case the main cause of the birefringence is not HIB, but simply the residual passive waveguide birefringence. In the dispersion compensator devices it causes a wavelength shift of the order of 0.05 nm which is substantial compared to the device FSR of 0.8 nm. It is very hard to reduce the passive birefringence of the waveguide further by process control alone. Therefore we decided to pursue another approach, where the polarization dependent wavelength shift of each delay line is trimmed to close to zero using UV irradiation.

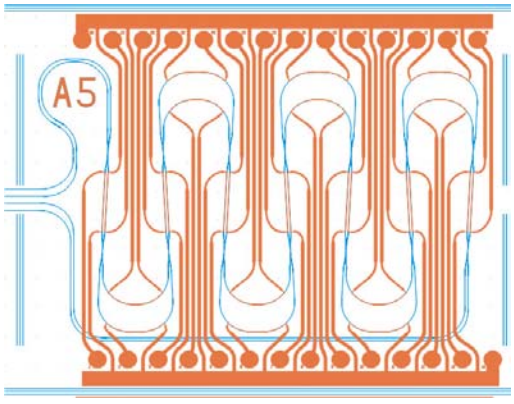

Fig. 4.2: Die layout of the Tunable Dispersion Equalizer. Die size is 16 x 12 mm

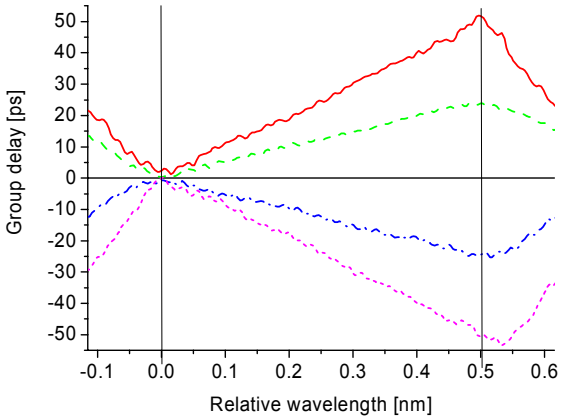

Fig. 4.3: Measured linear group delay curves for dispersion values of +100, +50, -50 and -100 ps/nm.

4.3. Trimming of residual birefringence

We found that irradiation of SiON waveguides with light pulses from an excimer laser at a wavelength of 193 nm produces a strong negative birefringence change in the waveguides, as demonstrated in Fig. 4.4. Using this effect, we can generate a section with opposite birefringence in each individual delay arm of the dispersion equalizer, thus minimizing the overall birefringence of the delay arm.

In order to finely trim the amount of compensating birefringence of a delay arm, the variable couplers before and after the delay arm were set to 3 dB coupling and all other couplers were set to zero coupling using the heaters on these couplers. In this way the dispersion compensator is reduced to a single Mach-Zehnder interferometer around the delay arm to be trimmed. While irradiating the delay arm, the shift of the TE and TM wavelength spectrum of the interferometer is continuously monitored, until the two spectra coincide. Examples of these Mach-Zehnder spectra, before and after trimming, are shown in Fig. 4.5. The trimming procedure is repeated for all 6 stages of the dispersion equalizer.

4.4. Results

The results that were achieved by UV trimming are documented by Figures 4.6 and 4.7. The first figure shows the delay curve for which the DGD values were measured. The DGD before trimming, as shown in Fig. 4.7, is approximately 4.5 ps in the usable band where the delay slope (= dispersion) is -120 ps/nm. Outside this band, which is indicated by the vertical dashed lines, both the return slope (Fig. 4.6) and the DGD (Fig. 4.7)

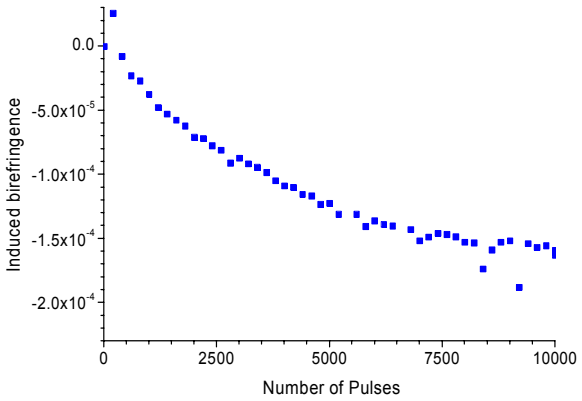

Fig. 4.4: UV-induced birefringence change in a SiON waveguide.

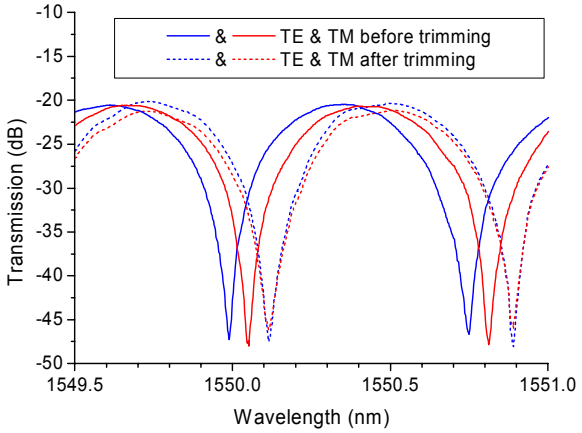

Fig. 4.5: UV-trimming of one stage of a dispersion equalizer.

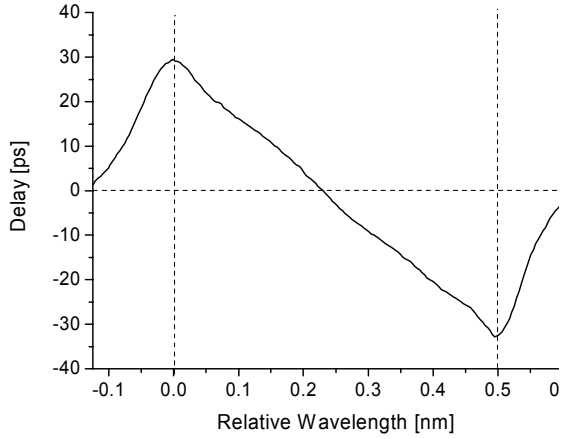

Fig. 4.6: Delay curve for a dispersion of -120 ps/nm. This setting was used for measuring DGD values.

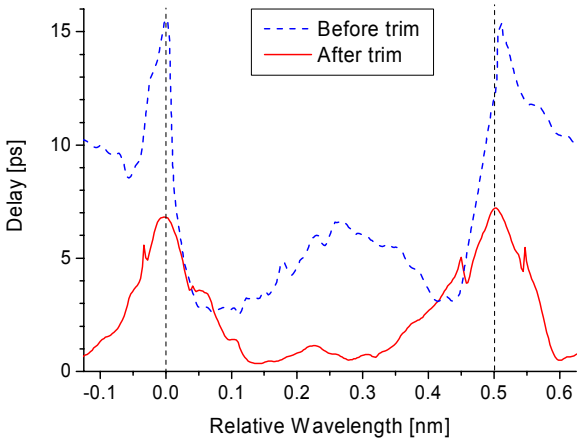

Fig. 4.7: DGD, measured before and after delay line birefringence trimming.

are about twice as large. This can well be explained by a DGD that is dominated by a polarization dependent wavelength shift of 0.35 nm.

After trimming, the DGD in the center of the usable band is strongly reduced to less than 1 ps. The regions with residual DGD now coincide with the extrema of the delay curve, where the curve shape is most sensitive to variations in the variable coupler settings. This residual DGD is probably the result of polarization dependent coupling in the variable couplers, which could be the result of HIB in the variable coupler heater waveguides, or polarization dependent coupling in the directional couplers. Both were not optimized in this device.

5. INTEGRATED OPTICAL POLARIZATION CONVERTER

5.1. Polarization conversion

One of the simplest ways to achieve a rotation of the input polarization of a beam of light by 90° is to place a half-wave-plate in the beam, with its fast and slow axes rotated by 45° relative to the input state of polarization. The input beam is then decomposed into two equally large components along the fast and slow axes of the waveplate. On propagation through the waveplate, the slow component acquires a phase delay of half a wavelength and is at the end effectively 'inverted' relative to the fast component. The re-addition of the two components then yields a polarization vector that is mirrored along the fast axis of the waveplate, and is thus effectively 'rotated' by 90°.

If, for some reason, a birefringence axis tilt of a full 45° can not be reached, polarization rotation can also be achieved with multiple half-wave-plates at lower tilt angles. For example, take two plates at +22.5° and −22.5°. The first plate flips the 0° input polarization state to +45°. The second plate flips this input state along the −22.5° waveplate axis to −90°. An even lower tilt of the axes of the half-wave-plates can be compensated by taking more plates. However, increasing the number of wave plates comes at the cost of increased wavelength sensitivity and increased size of the polarization rotator.

5.2. Device layout

In order to achieve an integrated polarization converter in SiON technology, a waveguide section with sufficient birefringence and tilted birefringence axes must be fabricated. As mentioned before in Sec. 2.5, this can be done by using a trench on only one side of the waveguide [3]. Fig. 5.1 shows the measured axis tilt, measured on a number of waveguides with single trenches at varying distances. The measurement shows that quite high values for the axis tilt, up to 35° can be achieved. However, to reach these high values, the trench must be close to the waveguide, with high risk to disrupt the mode field. Also, the dependency of tilt on trench distance is very steep in this region, which would make device performance very sensitive to process

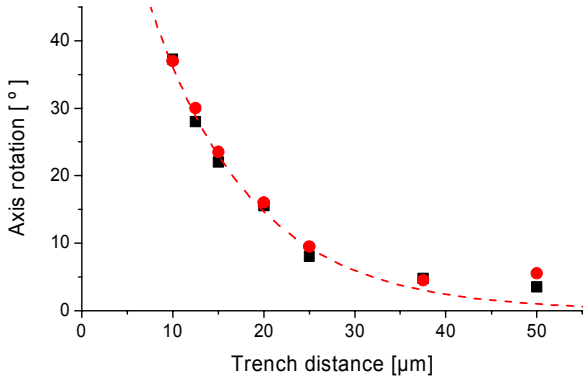

Fig. 5.1: Measured tilt of the birefringence axes of a waveguide with a trench on one side.

Fig. 5.2: Four-stage polarization converter using trenches at alternating sides of the waveguide.

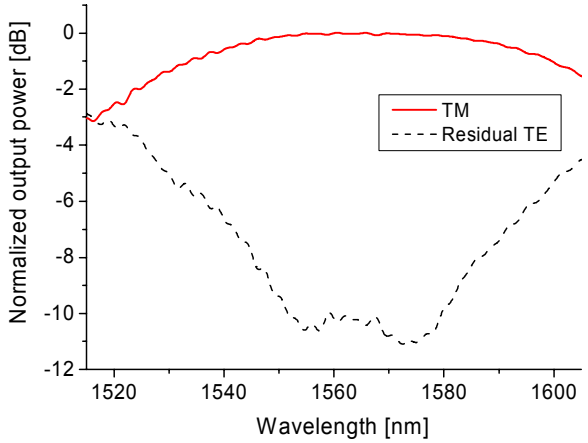

Fig. 5.3: Measured polarization conversion of a 4-stage device. Input polarization is TE.

variations. It was therefore decided to concentrate on 4 stage devices, which need only 11.25º of axis tilt and should have better reproducibility. A schematic drawing of such a device is shown in Fig. 5.2. The variation with wavelength of a 4 stage device is still quite low within the telecommunication window around 1550 nm.

5.3. Results

Fig. 5.3 shows measurement results on one of the 4 stage polarization rotator devices. The measurements show that in this device the suppression of residual TE is of the order of -11 dB, which is probably due to too high birefringence axis tilt (13.5º). Also the birefringence in the trench waveguides was much higher than expected leading to strongly increased phase delays. The device shown here is still functional because the phase delay per stage is 3 π rad. instead of only π. However, the larger phase delay leads to a stronger wavelength dependency that is clearly visible in the measured curve. The device shown here has 5 mm long trenches per stage. The optimum trench length would have been 1.6 mm, which would have yielded less wavelength sensitivity and a much shorter device.

6. POLARIZATION SPLITTER

6.1. Polarization splitter based on a single Mach-Zehnder interferometer

By etching trenches at both sides of a waveguide, the balance between stress-induced and geometrical birefringence is disrupted and the resulting waveguide section has considerable birefringence, as discussed in Section 4.3. This birefringence is relatively insensitive to the distance between the trenches and the trench width. Also, compared to a waveguide without trench, mainly TM-polarized light experiences a change in effective index of refraction. TE-polarized light is hardly affected.

Using an approximately 2mm long trench section, a phase delay of π radians between TE and TM polarized waves can be produced. This can be used in an integrated optical Mach-Zehnder interferometer to separate the TE and TM polarized light input light to the two different outputs, as depicted in Fig. 6.1.

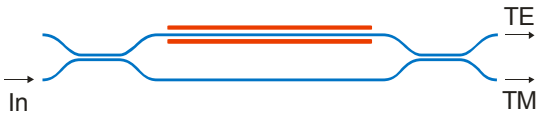

Fig. 6.1: Polarization splitter, based on a symmetric Mach-Zehnder interferometer with trenches etched along one arm.

Measurement results of a Mach-Zehnder polarization splitter are shown in Fig. 6.2. Optimum cross coupling of TE polarized light, and thus minimal residual TE light in the TM output, occurs when both directional couplers couple exactly 50%. For the measured device, this situation is approached at a wavelength of 1590 nm, which yields very small TE residual values of close to −25 dB. However, due to wavelength dependency of the directional couplers, the TE residual suppression deteriorates at higher and lower wavelengths.
Optimum coupling of TM polarized light to the bar output depends on the equality of the two directional couplers, which is easily achieved, and on the accuracy of the polarization dependent phase shift, generated by the trenches. In the original device, the trenches were slightly too long, resulting in the TM residual curve at the cross output given by the dotted line in Fig. 6.2. By adding 100 µm of trench on the other waveguide branch, the trench was effectively 'shortened', leading to the much improved TM residual curve, given by the dashed line.

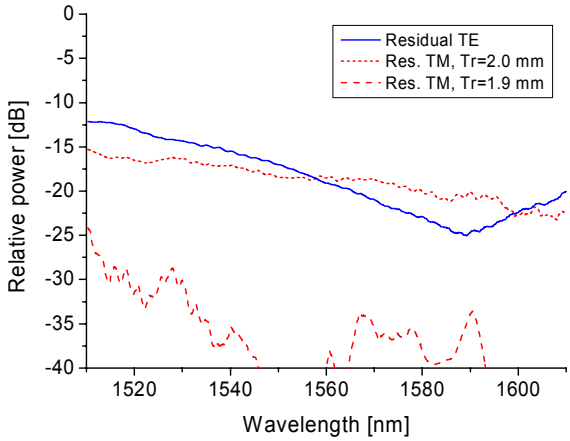

Fig. 6.2: Polarization splitting measurement results of the single Mach-Zehnder interferometer.

6.2. Two-stage polarization splitter

Although the trimmed Mach-Zehnder polarization splitter performs quite well, it also shows the disadvantages of this design: strong wavelength sensitivity of TE residual suppression, and strong trench length sensitivity of TM residual suppression. A possible solution for these disadvantages is to combine three polarization splitter stages, as shown in Fig. 6.3. Here, the first stage functions as the actual splitter and the two second stages function as post-filters. By tuning the directional couplers of the first and second stages for different wavelengths, a wide wavelength band with strong TE residual suppression can be generated. Likewise, by using slightly different lengths for the trenches in the two stages, a wider process window with strong TM residual suppression is achieved.

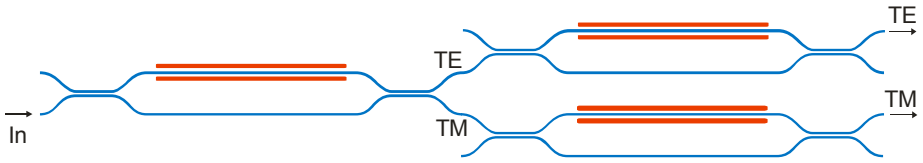

Fig. 6.3: Extended polarization splitter, using two added post-filter stages.

Measurement results for a polarization splitter based on this principle are shown in Fig. 6.4. The device performs quite well, although the single stages in this device are far from perfect, as confirmed by measurements on monitor ports.

The wavelength for minimum residual TE light for the first stage is tuned to below the measurement window, but still the extra residual suppression is visible in the flattening of the Residual TE curve below 1560 nm, and in the generally increased TE residual suppression.

In both stages the suppression of residual TM light is of the order of 10 dB due to imperfect length of the trenches. However, the TM suppression of the two stages together reaches 20 dB, which demonstrates the robustness of the two-stage approach.

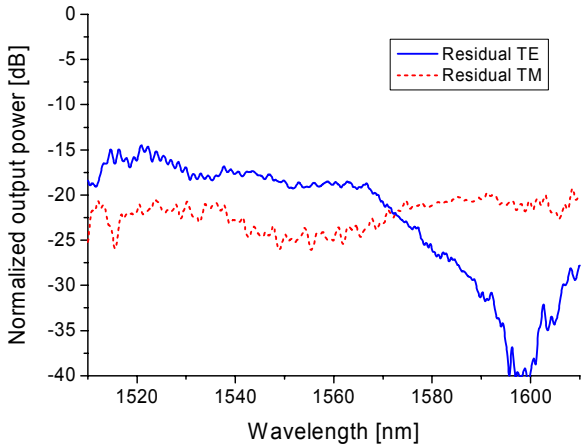

Fig. 6.4: Polarization splitting results of a double filtering Mach-Zehnder polarization splitter.

7. SUMMARY AND CONCLUSIONS

In this paper we describe a number of methods to control and manipulate waveguide polarization and birefringence in SiON waveguides, together with examples of the application of these methods.

The etching of trenches along waveguides proves to be the most versatile way to control and manipulate polarization effects. We have used trenches at both sides of tuning heaters to reduce the heater induced birefringence in a dynamic gain equalizer. Also, trenches at both sides of a waveguide were used to generate the specific amount of birefringence, needed to separate TE and TM polarized light in an integrated optical polarization splitter. And, using a trench at only one side of the waveguide, we could generate the integrated optical equivalent of a tilted half-wave-plate, which we used to fabricate an integrated optical polarization converter.
Furthermore, the birefringence in the waveguides also can be manipulated using a stressor layer on top of the waveguide. We showed that the waveguide heater can be used in this way, and if it is designed correctly it can even compensate the dynamic heater induced birefringence.
Lastly, in cases where very precise manipulation of the birefringence is needed, post-fabrication trimming of SiON waveguides is possible, using UV irradiation with an excimer laser. This was demonstrated by the PMD reduction in a tunable dispersion equalizer.

As demonstrated by the examples, all methods together provide a versatile toolbox that enables the fabrication, in SiON technology, of both devices with very low polarization sensitivity, for polarization independent systems, and devices that are deliberately strongly sensitive to polarization, for polarization separation and manipulation.

REFERENCES

1 G.L. Bona, R. Germann, B.J. Offrein, "SiON high-refractive-index waveguide and planar lightwave circuits," *IBM J. Res. Dev.*, **47**, No. 2/3, pp. 239-249, 2003.

2 Y. Inoue, K. Katoh, M. Kawachi, "Polarization sensitivity of a silica waveguide thermo-optic phase shifter for planar lightwave circuits," *IEEE Photon. Technol. Lett.*, **4**, no 1, pp. 36-38, Jan. 1992.

3 M. Kawachi, “Silica waveguides on silicon and their application to integrated-optic components,” *IEEE J. Opt. and Quantum Electron.*, **22**, pp. 391-416, 1990.

4 B.J. Offrein, F. Horst, G.L. Bona, R. Germann, H.W.M. Salemink, R. Beyeler, "Adaptive gain equalizer in high-index-contrast SiON technology," *IEEE Photon. Technol. Lett.*, **12**, no. 5, pp. 504-506, May 2000.

5 S.E. Harris, E.O. Ammann, and I.C. Chang, “Optical network synthesis using birefringent crystals,” *J. Opt. Soc. Amer.*, **54**, pp. 1267-1279, 1964.

6 K. Jinguji and M. Kawachi, “Synthesis of Coherent Two-Port Lattice-Form Optical Delay-Line Circuit,” *J. Lightwave Technol.* **13**, pp. 72-82, 1995.

7 K. Takiguchi, K. Jinguji, K. Okamoto, and Y. Ohmori, “Dispersion compensation using a variable group-delay dispersion equalizer,” *Electron. Lett.*, **31**, pp. 2192-2194, 1995.

8 F. Horst, R. Germann, U. Bapst, D. Wiesmann, B.J. Offrein and G.L. Bona, "Compact tunable FIR dispersion compensator in SiON technology," *IEEE Photon. Technol. Lett.*, **15**, no. 11, pp. 1570-1572, Nov. 2003.